JACS
JOURNAL OF THE AMERICAN CHEMICAL SOCIETY
pubs.acs.org/JACS

Open Access
This article is licensed under CC-BY-NC-ND 4.0

Article

Ballistic Conductance through Porphyrin Nanoribbons

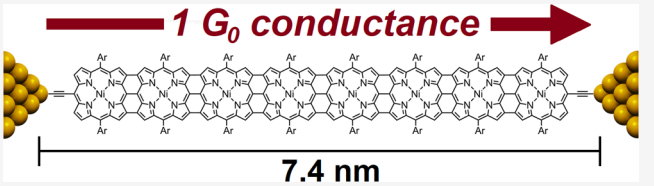
Jie-Ren Deng, M. Teresa González, He Zhu, Harry L. Anderson,* and Edmund Leary*

Cite This: https://doi.org/10.1021/jacs.3c07734

Read Online

ACCESS | Metrics & More | Article Recommendations | Supporting Information

ABSTRACT: The search for long molecular wires that can transport charge with maximum efficiency over many nanometers has driven molecular electronics since its inception. Single-molecule conductance normally decays with length and is typically far below the theoretical limit of G_0 (77.5 μS). Here, we measure the conductances of a family of edge-fused porphyrin ribbons (lengths 1−7 nm) that display remarkable behavior. The low-bias conductance is high across the whole series. Charging the molecules *in situ* results in a dramatic realignment of the frontier orbitals, increasing the conductance to 1 G_0 (corresponding to a current of 20 μA). This behavior is most pronounced in the longer molecules due to their smaller HOMO−LUMO gaps. The conductance-voltage traces frequently exhibit peaks at zero bias, showing that a molecular energy level is in resonance with the Fermi level. This work lays the foundations for long, perfectly transmissive, molecular wires with technological potential.



Downloaded via UNIV AUTONOMA DE MADRID on February 6, 2024 at 15:58:27 (UTC).
See https://pubs.acs.org/sharingguidelines for options on how to legitimately share published articles.

INTRODUCTION

The inefficiency with which molecular junctions transport charge over distances longer than 1−2 nm is a key problem hindering the development of electronic circuits based on single molecules or monolayers.[1,2] Studies on families of conjugated wires, predominantly connected between gold electrodes, generally show that conductance drops exponentially with distance, following the form

$$G(L) = Ae^{-\beta L} \quad (1)$$

where L is the molecular length, A is a prefactor (which can be viewed as a contact resistance), and β is the conductance attenuation factor describing how the conductance, G, decays with oligomer length.[3−6] The main reason for the exponential decrease is an energy mismatch between the transporting molecular orbitals and the electrode Fermi level (E_F). In many experiments, E_F is found to lie close to the center of the HOMO−LUMO gap, as demonstrated by the small voltage dependence of G around 0 V and the typically low Seebeck coefficients.[7−10] Although the HOMO−LUMO gap shrinks as the length of the π-conjugated oligomer increases, the greater tunneling distance tends to dominate, producing an exponential decay. For many π-conjugated chains, such as oligophenylene ethynylenes,[11] oligofluorenes,[12] oligoynes,[13,14] and oligoenes,[15] β lies in the range 2−4 nm^{-1}, G decaying 10−50 times with each additional nanometer. This is a huge problem because molecules longer than 3−4 nm become too resistive for single-molecule measurements.

Families of molecules that show a large decrease in the HOMO−LUMO gap with length can lead to β values close to zero. For example, π-conjugated oligomers with negligible bond-length alternation can have slightly positive or slightly negative β values. Examples include cumulenes,[16,17] oligomethines,[18,19] oxidized oligophenylene bis(triarylamines),[20] and oligo[n]emeraldines.[21,22] In these cases, however, the chemical stability usually drops rapidly with length, and it will be hard to use these materials in future componentry. Furthermore, a symmetry-breaking Peierls transition occurs beyond a critical length in highly symmetric molecules leading to conductance decay.[19,20] Such limitations call for different strategies for producing long, stable, and maximally conducting junctions.

π-Conjugated porphyrin oligomers are excellent wires due to their efficient π-overlap, stability, rigid frameworks, and small reorganization energies.[23] We recently showed that edge-fused porphyrins with up to three porphyrin subunits, connected to gold through thiolate groups, display ultralow β values at low bias[3] as a consequence of the rapidly decreasing HOMO−LUMO gap with length, which counters the greater tunneling distance. Remarkably, β becomes negative above ∼ 0.7 V, and hence G increases with length. For the fused trimer, at 0.7−0.8 V, $G \approx 10^{-2}$ G_0, which is a factor 100 times greater than at low bias. As V_{bias} was increased further, the conductance tended to level off, suggesting alignment between one of the frontier molecular orbitals and E_F and, thus, a resonant-tunneling regime. In this regime, individual molecules have been shown to become charged, as demonstrated by hysteresis in successive bias sweeps.[24] This underexplored phenomenon has only been reported for a few systems.[25,26] It is significant that the charged molecule can maintain high conductance even as the bias is

Received: July 19, 2023
Revised: November 22, 2023
Accepted: November 22, 2023

ACS Publications
© XXXX The Authors. Published by American Chemical Society

https://doi.org/10.1021/jacs.3c07734
J. Am. Chem. Soc. XXXX, XXX, XXX−XXX

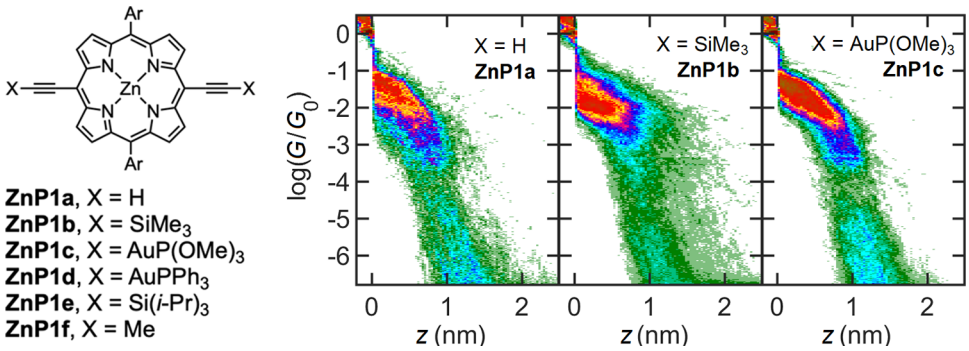


Figure 1. Model compounds for testing attachment to gold. Chemical structures of monomers **ZnP1a–f** (Ar = 3,5-bis(*t*-butyl)phenyl) and 2D histograms of the high-conductance traces of **ZnP1a–c**. The numbers of traces in the high-conductance group are 344 (6.6%) for **ZnP1a**, 1299 (6.5%) for **ZnP1b**, and 686 (6.5%) for **ZnP1c**.

brought back to zero. This behavior can be rationalized in terms of a two-channel mechanism, as proposed by Migliore and Nizan, in which a fast, coherent channel determines the measured conductance, while a slow, hopping channel controls the charge state.[27,28] The second channel effectively acts as an *in situ* gate, altering the alignment of the levels. We found that the high-conductance states of thiolate-anchored porphyrins can be stable over many seconds (limited in our case by instrument drift), which suggests this could be a viable route to form long, stable, and highly conductive molecular wires and perhaps even molecular-memory devices. Other kinds of bias-driven molecular-memory effects are known and are discussed elsewhere.[29−31]

The aim of this project was to create long, highly conductive molecular junctions by combining two features: (i) a molecular wire with a low β-factor and (ii) an electronically transparent connection to the electrodes (i.e., high A; low contact resistance). The attachment of molecules to gold electrodes with covalent Au−C bonds has often been used to generate highly conductive junctions from short molecules.[32−34] In this study, we tested various methods for attaching alkynes to gold electrodes and found that trimethylsilyl (TMS, i.e., $SiMe_3$) alkynes provide suitable connections. TMS-alkyne substituents are convenient proto-anchor groups because they are stable and easy to synthesize. We investigated charge transport through a series of edge-fused porphyrin nanoribbons consisting of up to eight nickel-porphyrin units terminating in TMS-alkynes, with lengths up to 7.1 nm, and found that these molecules give surprisingly transmissive junctions, reaching 1 G_0.

RESULTS AND DISCUSSION

Model Studies and Selection of the TMS Anchor Group. Many alkyne derivatives have been reported to act as anchor groups in Au|molecule|Au break-junctions.[32,35−45] Sometimes the effectiveness of an anchor group depends on the type of molecular wire or experimental setup; so we tested porphyrin monomers **ZnP1a–f** (Figure 1, with X = H, $SiMe_3$, $AuP(OMe)_3$, $AuPPh_3$, $Si(i\text{-}Pr)_3$, and Me) to guide our choice of acetylene proto-anchor group for this study (see the Supporting Information for the synthesis of **ZnP1a–f**). Terminal alkynes (X = H) are known to adsorb covalently onto gold surfaces[46] and to provide low-resistance junctions in gold break-junctions.[32,35−37] On the other hand, some reports suggest that gold complexes, such as X = $AuP(OMe)_3$, give higher junction-formation probabilities.[32,38] We tested the binding ability of **ZnP1a–f** using the scanning tunneling microscope break-junction (STM-BJ) technique to form single-molecule junctions. (A full description of data collection and post-processing is given in Supporting Information Section 2.2.) Our results (Figures 1 and S22−S24 for conductance histograms) show that **ZnP1a–d** gave junctions with conductances of $\log(G/G_0) = -1.0$ to -3.0, which is much higher than for analogous porphyrins with 4-AcS-$C_6H_4C_2$ anchors ($G \approx 10^{-4}$ G_0, Figure S9).[3,47,48] Several conductance groups could be distinguished, as discussed below. In contrast, **ZnP1e** and **ZnP1f** (X = $Si(i\text{-}Pr)_3$ and X = Me) gave no detectable junctions (Figure S24). We concluded that **ZnP1b** (X = $SiMe_3$) is the most convenient acetylene proto-anchor group because it gives similar junctions to **ZnP1a**, **ZnP1c**, and **ZnP1d** while being the most stable and synthetically accessible.

Previous work has shown that TMS-alkynes chemisorb onto gold Au(111) surfaces in a perpendicular orientation[49] and that they can form effective Au|molecule|Au junctions.[32,39−43] Some authors have reported that TMS-alkynes need activating with tetrabutylammonium fluoride to form molecular junctions,[44,45] although this does not always seem necessary.[32] Here, we found that such activation was unnecessary. The similarity between the conductance histograms of **ZnP1a–d** and the high conductances of these junctions suggests that all four compounds give the same covalently bonded Au−C≡C− connections, with spontaneous loss of the TMS group, probably through reaction with traces of moisture catalyzed by nascent gold adatoms in the break-junction. This hypothesis is supported by the observation that the triisopropylsilyl (TIPS) group in **ZnP1e** does not give molecular junctions (in keeping with the results of Ferradás et al.)[42] because the Si−C bonds in TIPS-alkynes are generally much more robust than in TMS-alkynes. Further support for this is provided by the report that *tert*-butyl alkynes, $Me_3C-C\equiv C-$, do not form similar junctions as $Me_3Si-C\equiv C-$, despite the structural similarity.[40,42,51] It has been suggested that TMS-alkynes bind to gold via five-coordinate trigonal-bipyramidal silicon, Au-$SiMe_3-C\equiv C-$,[40,50] but this is not supported by computational results.[42] The observation that **ZnP1f** (X = Me) does not form junctions demonstrates that cleavage of the TMS group is required and that a side-on π-interaction alone is not sufficient to give a viable contact.

Synthesis and Characterization of Porphyrin Nanoribbons. The TMS-terminated porphyrin nanoribbons **NiP1**, **NiP2**, **NiP4**, **NiP6**, and **NiP8** were synthesized as shown in Figure 2a (see the Supporting Information for details). These oligomers were metalated with nickel(II), rather than zinc, to

https://doi.org/10.1021/jacs.3c07734
J. Am. Chem. Soc. XXXX, XXX, XXX−XXX

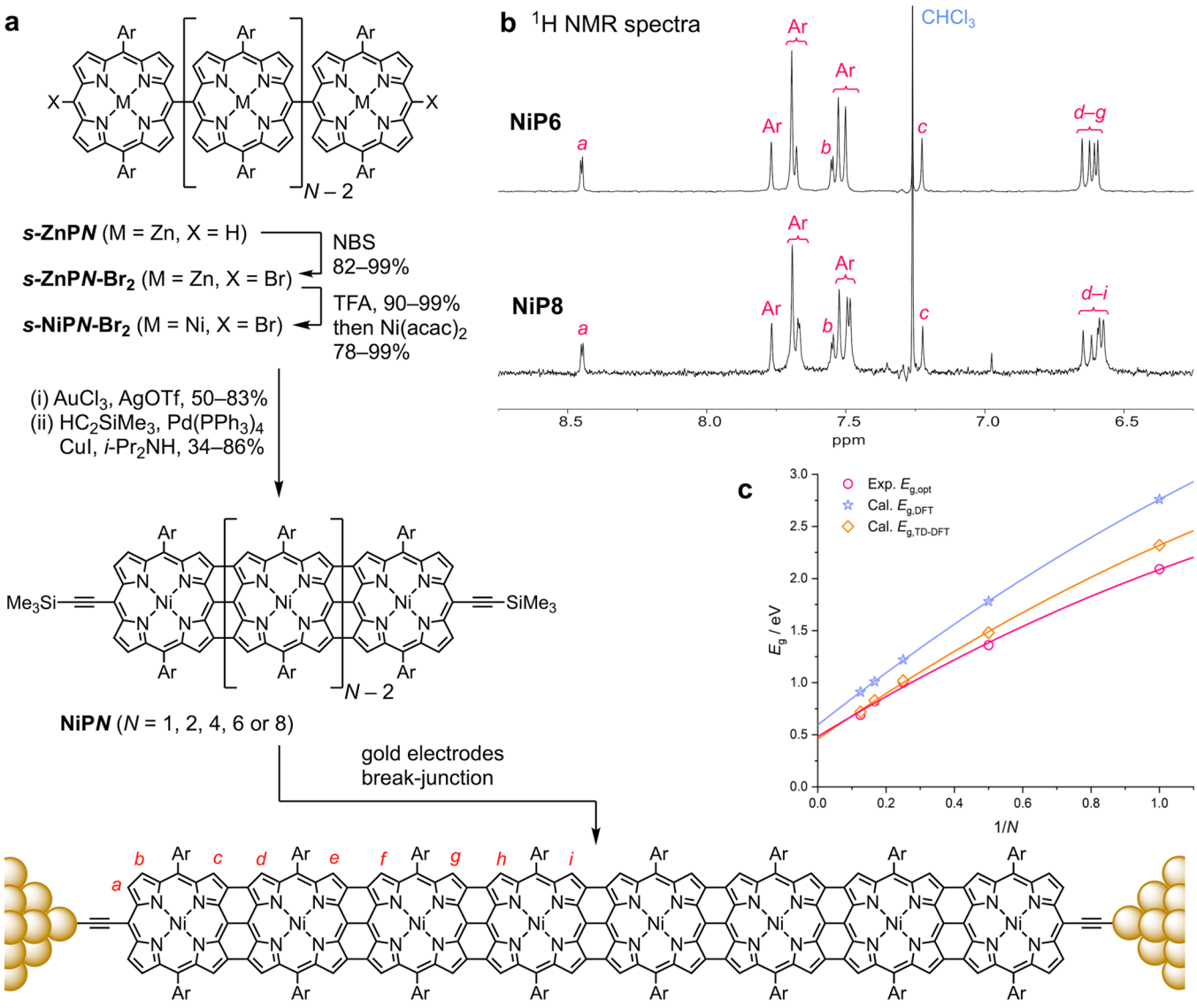


Figure 2. Synthesis and characterization of porphyrin nanoribbons. (a) Synthesis of **NiP1**−**NiP8** and schematic of **NiP8** forming a molecular junction. Ar = 3,5-bis(tri-*n*-hexylsilyl)phenyl. (b) Partial ^{1}H NMR spectra of **NiP6** and **NiP8** ($CDCl_3$, 298 K, 700 MHz; diffusion edited). (c) HOMO−LUMO gaps of **NiP1**, **NiP2**, **NiP4**, **NiP6**, and **NiP8** plotted against $1/N$.

make them more resistant to accidental oxidation. *Meso*-3,5-bis(tri-*n*-hexylsilyl)phenyl substituents were used to avoid aggregation and achieve high solubility. The bulky side chains probably also prevent the flat faces of the porphyrins from adsorbing onto gold surfaces. Treatment of the singly-linked oligomers, *s*-**ZnPN**, with *N*-bromosuccinimide resulted in efficient bromination of the terminal *meso*-positions to yield *s*-**ZnPN-Br$_2$**. The coordinated metal was then changed to nickel(II) before oxidative fusion and Sonogashira coupling with TMS-acetylene. The presence of nickel(II) makes it necessary to use harsher conditions in the oxidative fusion step ($AuCl_3$/AgOTf)[51] than would have been required for zinc(II) porphyrins. The well-resolved ^{1}H NMR spectra (Figure 2b) and MALDI-ToF mass spectra (Supporting Information) confirm the purity, solubility, lack of aggregation, and absence of accidental oxidation in these compounds.

The UV−vis−NIR absorption spectra of **NiP1**, **NiP2**, **NiP4**, **NiP6**, and **NiP8** illustrate the dramatic reduction in the HOMO−LUMO gap with length, as reported previously for similar edge-fused porphyrin nanoribbons.[52,53] The transition energies of the longest wavelength absorption maxima ($E_{g,opt}$ measured in $CHCl_3$ at 298 K) are plotted against $1/N$ in Figure 2c, showing a good fit to eq 2, which can be derived from a simple particle-in-a-box model, where N is the number of repeat units and a, b, and c are empirical parameters.[54]

$$E_g = a + b\frac{1}{N} + c\frac{1}{N^2} \quad (2)$$

Electrochemical measurements were also performed on **NiP1**, **NiP2**, and **NiP4** (Supporting Information pages S33−S35). From these, it is possible to extrapolate an energy gap of the infinite polymer, which gave a value of 0.47 eV. Energy gaps from density functional theory (DFT) calculations ($E_{g,DFT}$) and transition energies from time-dependent DFT ($E_{g,TD\text{-}DFT}$), also shown in Figure 2c, match well with the experimental data (B3LYP/6-31G* level of theory; PCM solvent model, $CHCl_3$). The parameter a from the UV−vis−NIR data provides an estimate of the gap for the infinite polymer of 0.48 eV ($E_{g,opt}$; from the longest wavelength absorption maxima, which is very similar to the electrochemi-

https://doi.org/10.1021/jacs.3c07734
J. Am. Chem. Soc. XXXX, XXX, XXX−XXX

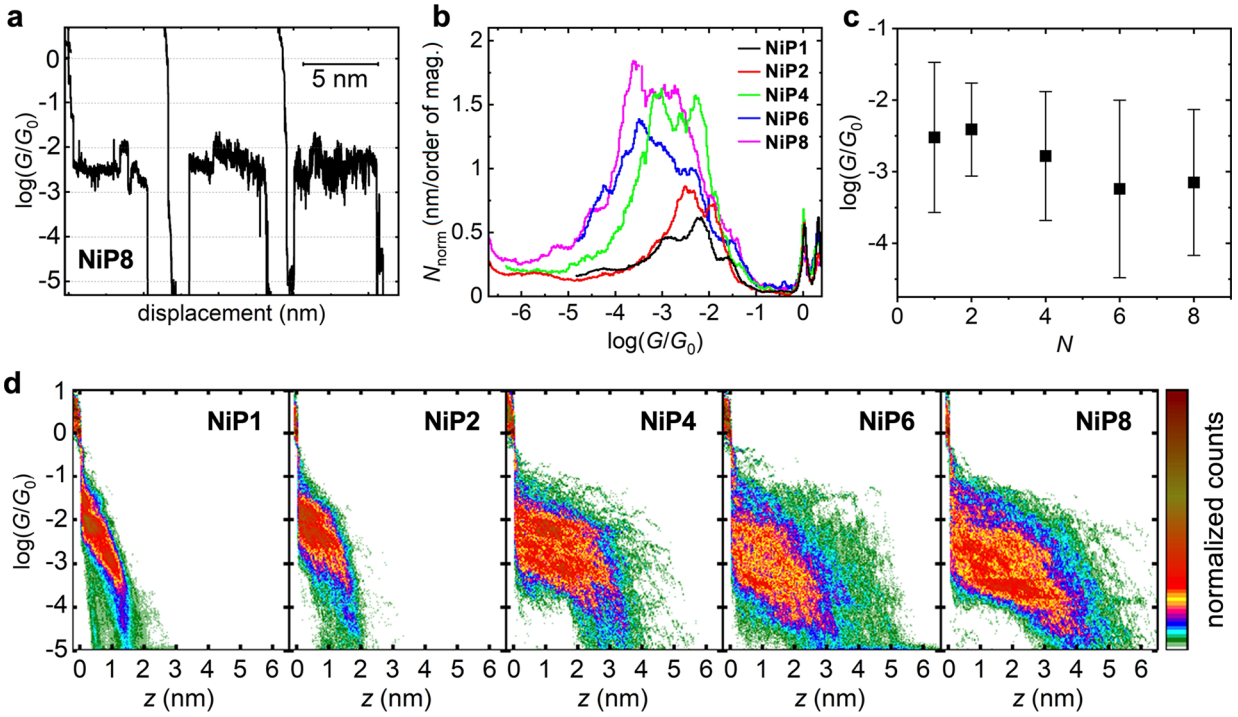


Figure 3. (a) Examples of individual conductance vs distance (G-z) traces for **NiP8**. (b) 1D conductance histograms of **NiP1** to **NiP8** after removing background tunneling traces and very short plateaus. The values were determined from a single Gaussian peak fit to each histogram. (d) 2D conductance−distance histograms of **NiP1** to **NiP8**.

cally derived value). This compares to 0.59 eV ($E_{g,DFT}$; from the DFT calculated HOMO−LUMO gaps) and 0.46 eV ($E_{g,TD\text{-}DFT}$; from the TD-DFT calculated optical transitions).

Conductance Measurements on Porphyrin Nanoribbons. We used the STM-BJ technique to form single-molecule junctions of **NiP1**−**NiP8** under ambient conditions in the absence of a solvent (see Supporting Information Section 7 for further details). The conductance of each compound was measured both at fixed low bias (0.2 V, Figure 3) and as a function of voltage between ±1.0 V. For each compound, we initially separated plateau-containing G-z traces from those with only background tunneling using an algorithm that searches for regions of constant conductance. Following this, we performed a k-means clustering analysis to remove very short plateaus (probably) arising from unsuccessful attachments. The conductance of **NiP1** lies in the range $\log(G/G_0)$ = −1.5 to −3.5, and the conductance histograms display three significant peaks (Figure 3b black curve) which we designate high, medium, and low (H, M, L, see Supporting Information Figure S5 for a labeled histogram). The k-means clustering analysis (Supporting Information Section 7.3) suggests that L corresponds to the fully-stretched junction, while M and H originate from compressed forms of the junction, which might be caused by differing degrees of π-overlap between the triple bond and the gold electrodes (Supporting Information Figure S8).

The 1D histogram of **NiP2** (Figure 3b) is in the same conductance range as **NiP1**, but the G-z plateaus are correspondingly longer (see the 2D histograms in Figure 3d). There are two prominent peaks, with a third smaller peak on the low conductance side. For **NiP4**, the three-peak structure is still present, although there is a general shift to slightly lower conductance values and the histogram broadens. **NiP6** and **NiP8** continue this trend, displaying greater weight at yet lower conductance values, and the three-peak structure is no longer visible. The 2D histogram of **NiP8** (with a molecular length over 7 nm) shows that junctions with conductance values above $\log(G/G_0)$ = −3 typically extend to inter-electrode separations of 3.5−4.5 nm (after the gold snap-back is accounted for). The lower conducting junctions extend to between 4.5 and 5.5 nm, which approaches the maximum distance expected. To quantify the conductance for each compound, and determine a β value, we fitted each histogram with a single Gaussian curve that encompasses the entire conductance range, ignoring the discrete peaks. A linear fit to the natural logarithm of G (Supporting Information Figure S10) gave a β value of 0.33 (±0.08) nm^{-1}, which is much lower than typical organic oligomers but similar to the value for short thiolate porphyrin nanoribbons (0.5 nm^{-1}).[3]

The behavior of **NiP1**−**NiP8** changes dramatically at higher bias voltages. We performed current vs voltage (I-V) ramps in the range ±1.0 V. For **NiP1**, all $\log(G/G_0)$-V traces (where $G = I/V$) show a slight increase in conductance of $\Delta\log(G/G_0)$ = 0.2 between 0.0 V and ±1.0 V (Figure 4a, see Supporting Information Figure S11a for individual examples) and have a U-shape characteristic of off-resonant tunneling.[55] The small increase shows that the closest molecular level is energetically far from E_F. The picture changes with **NiP2**, where only ∼50% of the $\log(G/G_0)$-V traces are U-shaped. The low−high bias conductance increase is greater than that of **NiP1** due to its smaller HOMO−LUMO gap (see Figure 2c for a plot of the HOMO−LUMO gap for each compound). The other 50% are different, having, for example, a 'V' shape (see Supporting Information Figure S11c for examples) which indicates that molecules are charging due to the bias.[24] This becomes possible due to the rapidly decreasing HOMO−LUMO gap with length (see Figure 2c and Supporting Information Figure S2 for the UV−vis−NIR and electrochemically-derived energy

https://doi.org/10.1021/jacs.3c07734
J. Am. Chem. Soc. XXXX, XXX, XXX−XXX

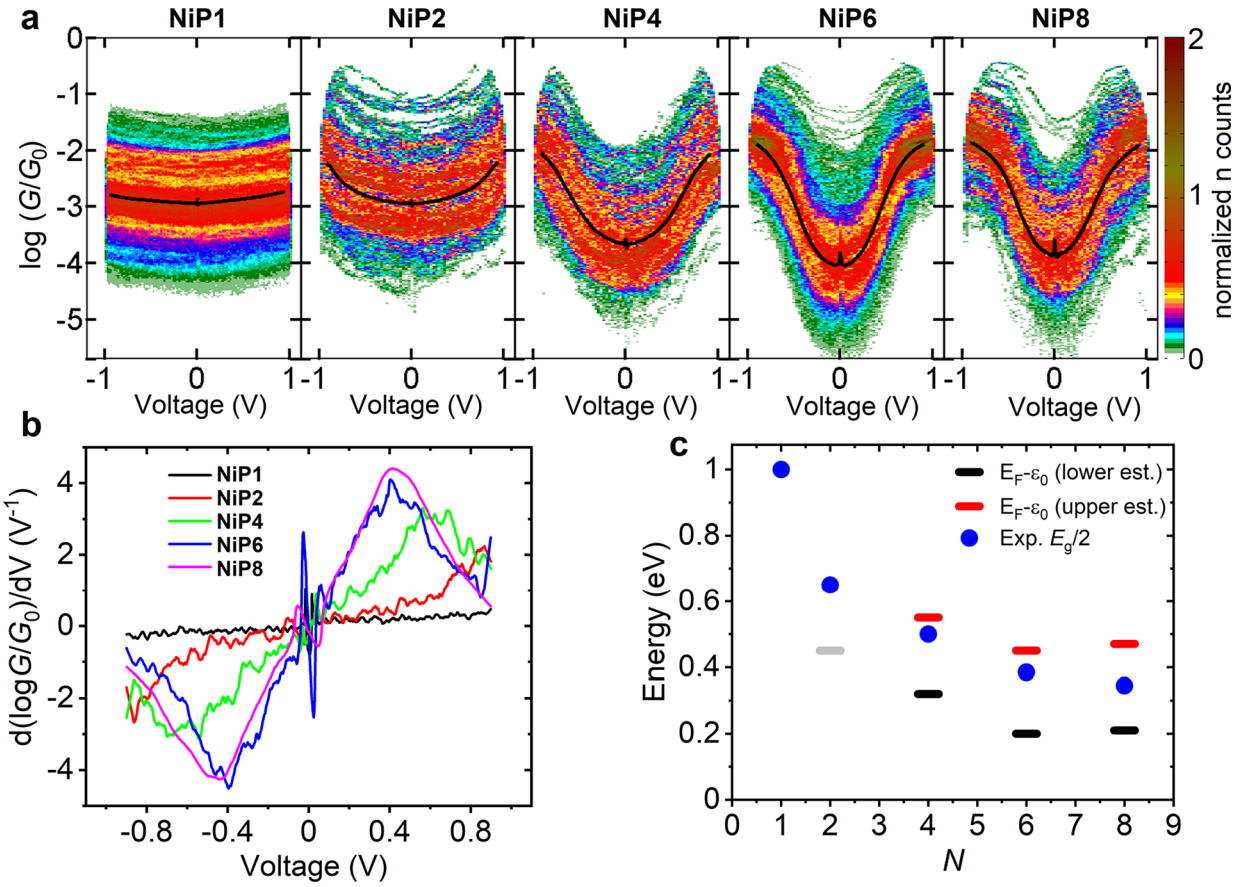


Figure 4. (a) Log(G/G_0)-V histograms for each molecule, generated by combining all of the individual log(G/G_0)-V traces from the recorded molecular junctions. The black lines are the mean log value. (b) First derivative of the mean U-shaped log(G/G_0)-V trace (which are the black lines) superimposed on the 2D histograms in (a). (c) Estimated position of ε_0 based on the d(logG/G_0)/dV curves compared to half of the optical HOMO−LUMO gaps (blue circles). The gray line for N = 2 is a guess as we do not clearly observe a maximum in d(logG/G_0)/dV for this compound.

gaps respectively). For the longer **NiP4**−**NiP8** wires, the percentage of U-shaped traces further decreases to between 5 and 15% and, for **NiP6** and **NiP8**, many level off at high bias (Supporting Information Figure S11b). We manually extracted the non-hysteretic U-shaped traces, which are shown as 2D histograms in Figure 4a (no separation was necessary for **NiP1**).[56] The shrinking HOMO−LUMO gap can be inferred by the increasing degree of curvature and steepness, indicating that the closest molecular level approaches E_F as the length of the oligomer increases. For a single molecular level (ε_0) equally coupled to two electrodes, a maximum in dI/dV would be expected when ε_0 aligns with the chemical potential of either electrode.[55] We found individual, low noise junctions with peaks in dI/dV (Supporting Information Figure S16); however, maxima in the average dI/dV trace were not very clear (Supporting Information Figure S17), which could suggest a degree of averaging-out of detail. Some deviation from ideal single-level behavior may occur if E_F sits close to the center of the HOMO−LUMO gap, causing both levels to contribute to transport. Closely spaced levels beyond the frontier orbital which come into play at high bias (as suggested from our electrochemical study) may also lead to deviations from the ideal single-level picture in this regime. Interestingly, plots of d(logG/G_0)/dV (Figure 4b) show clear peaks (for **NiP4**−**NiP8**) which drop toward zero at higher bias (**NiP6**−**NiP8**). Plotting the corresponding energy shift of the chemical potentials (E = eV/2) at the peak (black bars, Figure 4c) and zero−crossing points (red bars, obtained by extrapolating to zero) more easily allows us to approximate the position of ε_0. The blue circles show the gaps obtained from our UV−vis−NIR measurements. For further comparison, we fitted the overall average I-V curve, as well as a selection of individual I-V curves for **NiP8**, using the temperature-dependent single-level model (SLM, Supporting Information Figures S14 and S15).[55,57] Extracted parameters for the average trace were $\Gamma_{left/right}$ = 1.6 meV and $E_F - \varepsilon_0$ = 0.32 eV, which fits with the estimated position above. Again, better fits were obtained for individual traces, which gave values of $E_F - \varepsilon_0$ between 0.29−0.35 eV. These results show overall that for each molecule, E_F likely sits close to the center of the HOMO−LUMO gap.

Figure 5a shows a reversible G-V trace (plotted as log(G/G_0)-V) for **NiP6** (black trace recorded first, followed by the red trace), in which the junction is brought smoothly into and out of resonance. The G-V curve starts leveling at ca. ± 0.6 V (i.e., in both bias sweeps) indicating ε_0 is within the bias window. Further increase of V_{bias} may thus bring more levels into resonance. Figure 5b,c shows the situation when a junction becomes hysteretic (in this case for **NiP8**). This is when voltage-induced charging takes place. The lack of hysteresis for **NiP1** also proves that the small HOMO−LUMO gaps in the longer oligomers facilitate charging during bias sweeps. The charged-state lifetime can vary, as seen by comparing panels b and c. Intriguingly, Figure 5d shows a new phenomenon that we have not previously observed. Initially, ε_0

https://doi.org/10.1021/jacs.3c07734
J. Am. Chem. Soc. XXXX, XXX, XXX−XXX

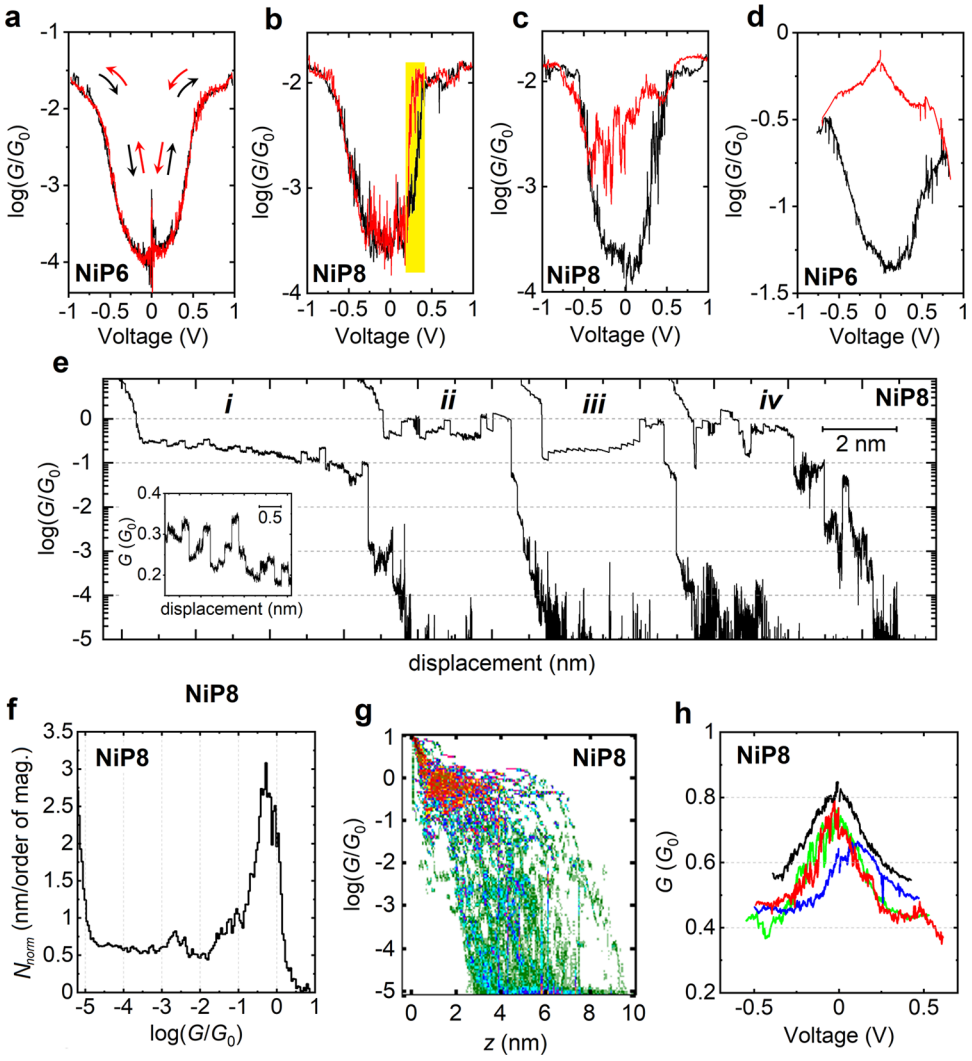


Figure 5. (a–d) Examples of log(conductance) vs voltage (log(*G*-*V*)) *sweeps recorded on molecular junctions of* ***NiP6*** *and* ***NiP8****. In each case, the black trace is recorded first (starting at −1.0 V) followed by the red trace (which starts at +1.0 V). Colored arrows indicate the direction of the bias sweep. (a) Reversible traces for* ***NiP6****. (b) Short-lived charged state for* ***NiP8*** *(hysteresis can be seen in the yellow-shaded region). (c) Long-lived charged state of* ***NiP8*** *in which the junction starts off-resonant (black trace), charges while under high bias, and then remains in the high-conductance state (red trace) but with significant fluctuations. (d) Junction that switches from off-resonant to on-resonant, showing a peak at zero bias. (e) Examples of ultraconducting charged molecular junctions of* ***NiP8****. The inset shows a magnified view of the left-hand trace showing periodic jumps in conductance that occur approximately every 2–3 Å. (f) 1D conductance histogram built from 60 of the most-conductive junctions. (g) 2D conductance-distance histograms from the same data. (h) Further examples of log(*G*/G_0)-*V* traces showing a peak at zero bias from junctions with conductances close to 1 G_0. Each example is taken from a separate molecular junction.*

sits within the bias window (black trace, starting at −0.7 V) where log(G/G_0) = −0.5 (0.3 G_0, i.e., a highly conducting junction). As V_{bias} is reduced, G drops rapidly, reaching a minimum between ±0.25 V, 10 times lower than on resonance, and then rises rapidly as ε_0 is again brought back into resonance. Around +0.7 V, however, the junction switches and the red return trace is completely different, showing a peak centered at 0 V. The conductance is now extremely high ($G_{0\,V}$ = 0.6 G_0, which is 30 times greater than in the black trace) and close to the maximum possible through a single molecular level.

We now focus on **NiP8** to describe this extraordinary high-bias behavior. We found 125 junctions (18% of the total) which, when the bias was swept between ±1.0 V, displayed low-bias conductances above 0.1 G_0 at distances >2 nm. We stress that when V_{bias} was restricted to 0.2 V, as in Figure 3, there was no significant signal above 0.01 G_0. Junction ***i*** (Figure 5e, data points taken at 0.2 V) begins at 0.3 G_0 and remains above 0.1 G_0 during stretching (∼7 nm). Of these junctions, 60 had conductances >0.5 G_0 beyond 2 nm and, strikingly, 23 showed conductances at, or just above, 1 G_0 (for example, junctions ***ii***–***iv*** in Figure 5e). We term junctions with G values >0.5 G_0 at distances beyond 2 nm ultraconducting (ultra-G) to distinguish their extraordinary behavior. We further note that we did not observe any ultra-G junctions for **NiP1** or **NiP2**, which again highlights the relation with a small HOMO–LUMO gap. Figure 5f shows the 1D histogram built from ultra-G junction which, on average, could be stretched 3–4 nm before breakdown (2D histogram, Figure 5g), similar to the neutral junctions. The inset of Figure 5e also shows a zoomed view of junction ***i*** highlighting periodic jumps in conductance at intervals of ∼0.25 nm, indicating atomic rearrangements. Such behavior underlines the importance of mechanically tuning the contact to obtain ultra-G junctions.

https://doi.org/10.1021/jacs.3c07734
J. Am. Chem. Soc. XXXX, XXX, XXX−XXX

We also observed much larger G jumps than previously seen at fixed low bias, between approximately 10^{-4} G_0 and 10^{-1} G_0, which we attribute to spontaneous charging events (Supporting Information Figure S20).

G-V curves recorded during evolution of ultra-G junctions varied, but remarkably 53 junctions displayed well-defined peaks in G at zero bias. In total, we recorded 118 individual $G-V$ traces of this type (6% of all the G-V traces recorded on ultra-G junctions, Figure 5h, see also Supporting Information Figure S19). We are unaware of this phenomenon in other room-temperature single-molecule junctions. Zero-bias peaks are expected for Kondo resonances,[58] but as we are well above the Kondo temperature previously measured for a porphyrin nanoribbon,[59] we rule this out. Instead, we attribute them to a near-perfectly aligned molecular orbital with E_F. The energy level schemes shown in Figure 6 provide an explanation. The

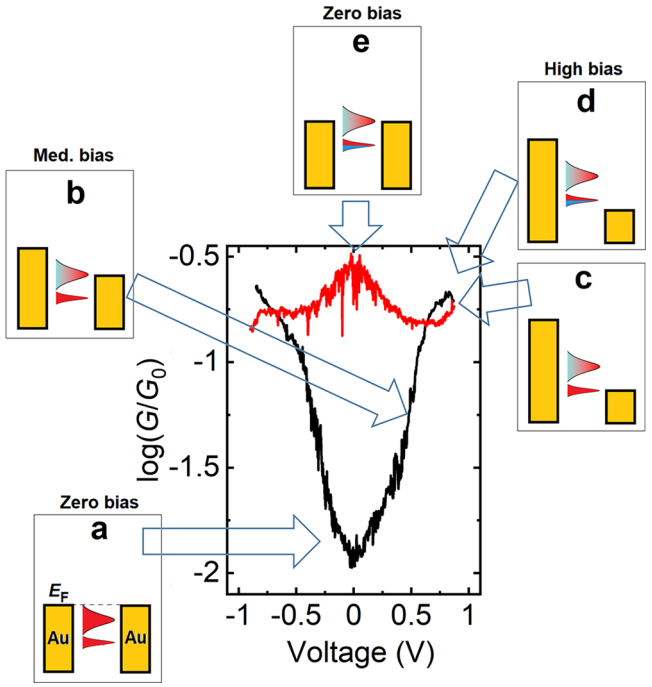


Figure 6. Energy level scheme to explain the hysteresis, G-V shapes, and ballistic conductance observed for the longer nanoribbons. Red represents a filled level, red and blue solid colors represent a partially filled level, and red and blue shading represent a level undergoing continuous filling and emptying. The large arrows indicate the approximate positions along the $\log(G/G_0)$-V traces that correspond to the energy level models. In panel (a), ε_0 is off-resonant. As the bias is increased, ε_0 is brought into resonance (panel b). Further increase in V_{bias} results in the weakly coupled level ε_{-1} coming into resonance (panel c) which undergoes charging via oxidation (panel d). This causes the molecular levels to shift upward in energy such that when the bias returns to zero (panel e), ε_0 now sits at (or close to) the Fermi level.

key ingredients are a well-coupled level (ε_0) responsible for the current and a weakly coupled level (ε_{-1}) responsible for charging. The HOMO of oligo(porphyrins) generally shows large weight at the *meso* positions which results in strong molecule-electrode coupling, while the HOMO−1 typically displays a node at this position and is, therefore, weakly coupled.[24] After charging, repositioning of the levels takes place (Figure 6c,d), where the final alignment of ε_0 (strongly coupled level) determines the precise shape of the G-V trace. When ε_0 aligns right at E_F, a peak in G appears. We compared a sequence of $\log(G/G_0)$-V traces in which transport switched from off-resonant to on-resonant with the SLM (Supporting Information Figure S19a,b). The SLM captures the dramatic change in the shape of the traces when ε_0 shifts. A zero-bias peak is only produced when ε_0 is closer than ∼0.05 eV. The zero-bias peak in Supporting Information Figure S18, for example, could be fitted with the following parameters: $\Gamma_{left/right}$ = 2 meV and $E - \varepsilon_0$ = 0.01 eV, showing that the coupling is in the same range after charging, but ε_0 now lies at E_F. This shows how molecules can behave like metal chains and conduct perfectly at low bias. This opens up the exciting possibility of moving beyond 10 nm in single-molecule conductance experiments.

CONCLUSIONS

We studied a family of edge-fused porphyrin nanoribbons up to 7.1 nm in length (8 porphyrin units) by using the STM-BJ technique. Low-resistance gold-acetylide contacts give large low-bias conductances up to 10^{-2} G_0 but also show that electron transport is still suppressed relative to an ideal system. Remarkably, bias-induced charging causes a dramatic realignment of the frontier orbitals, producing stable junctions with conductance up to 1 G_0. In this regime, we observed a new feature in conductance-voltage traces with peaks at 0 V, showing that a level lies right at the Fermi level. This study proves it is possible for molecular wires in the 5−10 nm range, with well-defined atomic binding groups, to have perfect electronic transmission. The challenge is now to explore the limits of this ballistic transport regime in molecules and also learn how to manipulate it.

ASSOCIATED CONTENT

Supporting Information

The Supporting Information is available free of charge at https://pubs.acs.org/doi/10.1021/jacs.3c07734.

Synthetic procedures, characterization data, UV−vis−NIR spectra, electrochemical measurements, DFT and TDFT simulations, STM-BJ measurements (PDF)

AUTHOR INFORMATION

Corresponding Authors

Harry L. Anderson − *Department of Chemistry, Chemistry Research Laboratory, Oxford University, Oxford OX1 3TA, U.K.*; orcid.org/0000-0002-1801-8132; Email: harry.anderson@chem.ox.ac

Edmund Leary − *Fundación IMDEA Nanociencia, 28049 Madrid, Spain*; orcid.org/0000-0001-7541-5997; Email: edmund.leary@imdea.org

Authors

Jie-Ren Deng − *Department of Chemistry, Chemistry Research Laboratory, Oxford University, Oxford OX1 3TA, U.K.*

M. Teresa González − *Fundación IMDEA Nanociencia, 28049 Madrid, Spain*; orcid.org/0000-0002-7253-797X

He Zhu − *Department of Chemistry, Chemistry Research Laboratory, Oxford University, Oxford OX1 3TA, U.K.*

Complete contact information is available at: https://pubs.acs.org/10.1021/jacs.3c07734

Notes

The authors declare no competing financial interest.

https://doi.org/10.1021/jacs.3c07734
J. Am. Chem. Soc. XXXX, XXX, XXX−XXX

■ ACKNOWLEDGMENTS

E.L. thanks the Comunidad de Madrid Atracción de Talento grant 2019-T1/IND-16384 and the Spanish MICIN (MCIN/AEI/10.13039/501100011033) PID2021-127964NB-C21. H.L.A. thanks the European Research Council (grant 885606, ARO-MAT). IMDEA Nanociencia acknowledges support from the 'Severo Ochoa' Programme for Centres of Excellence in R&D (CEX2020-001039-S). T.G. thanks NanomagCOST-CM (S2018/NMT-4321) and DECOSMOL (EIGConcertJapan).

■ REFERENCES

(1) Franklin, A. D. Nanomaterials in transistors: from high-performance to thin-film applications. *Science* **2015**, *349*, No. aab2750.
(2) Zhang, S.; Pang, J.; Li, Y.; Yang, F.; Gemming, T.; Wang, K.; Wang, X.; Peng, S.; Liu, X.; Chang, B.; Liu, H.; Zhou, W.; Cuniberti, G.; Rümmeli, M. H. Emerging internet of things driven carbon nanotubes-based devices. *Nano Res.* **2022**, *15*, 4613−4637.
(3) Leary, E.; Limburg, B.; Alanazy, A.; Sangtarash, S.; Grace, I.; Swada, K.; Esdaile, L. J.; Noori, M.; González, M. T.; Rubio-Bollinger, G.; Sadeghi, H.; Hodgson, A.; Higgins, S. J.; Lambert, C. J.; Anderson, H. L.; Nichols, R. J. Bias-driven conductance increase with length in porphyrin tapes. *J. Am. Chem. Soc.* **2018**, *140*, 12877−12883.
(4) Lafferentz, L.; Ample, F.; Yu, H.; Hecht, S.; Joachim, C.; Grill, L. Conductance of a single conjugated polymer as a continuous function of its length. *Science* **2009**, *323*, 1193−1197.
(5) Garner, M. H.; Li, H.; Chen, Y.; Su, T. A.; Shangguan, Z.; Paley, D. W.; Liu, T.; Ng, F.; Li, H.; Xiao, S. Comprehensive suppression of single-molecule conductance using destructive σ-interference. *Nature* **2018**, *558*, 415−419.
(6) Su, T. A.; Neupane, M.; Steigerwald, M. L.; Venkataraman, L.; Nuckolls, C. Chemical principles of single-molecule electronics. *Nat. Rev. Mater.* **2016**, *1*, 16002.
(7) Rincón-García, L.; Evangeli, C.; Rubio-Bollinger, G.; Agraït, N. Thermopower measurements in molecular junctions. *Chem. Soc. Rev.* **2016**, *45*, 4285−4306.
(8) Grace, I. M.; Olsen, G.; Hurtado-Gallego, J.; Rincón-García, L.; Rubio-Bollinger, G.; Bryce, M. R.; Agraït, N.; Lambert, C. J. Connectivity dependent thermopower of bridged biphenyl molecules in single-molecule junctions. *Nanoscale* **2020**, *12*, 14682−14688.
(9) Miao, R.; Xu, H.; Skripnik, M.; Cui, L.; Wang, K.; Pedersen, K. G.; Leijnse, M.; Pauly, F.; Warnmark, K.; Meyhofer, E. Influence of Quantum interference on the thermoelectric properties of molecular junctions. *Nano Lett.* **2018**, *18*, 5666−5672.
(10) Dell, E. J.; Capozzi, B.; Xia, J.; Venkataraman, L.; Campos, L. M. Molecular length dictates the nature of charge carriers in single-molecule junctions of oxidized oligothiophenes. *Nat. Chem.* **2015**, *7*, 209−214.
(11) Kaliginedi, V.; Moreno-Garcia, P.; Valkenier, H.; Hong, W.; Garcia-Suarez, V. M.; Buiter, P.; Otten, J. L. H.; Hummelen, J. C.; Lambert, C. J.; Wandlowski, T. Correlations between molecular structure and single-junction conductance: a case study with oligo(phenylene-ethynylene)-type wires. *J. Am. Chem. Soc.* **2012**, *134*, 5262−5275.
(12) Sagan, C.; Jiang, Y.; Caban, F.; Snaider, J.; Amell, R.; Wei, S.; Florio, G. M. Oligofluorene molecular wires: synthesis and single-molecule conductance. *J. Phys. Chem. C* **2017**, *121*, 24945−24953.
(13) Wang, C.; Batsanov, A. S.; Bryce, M. R.; Martin, S.; Nichols, R. J.; Higgins, S. J.; Garcia-Suarez, V. M.; Lambert, C. J. Oligoyne single molecule wires. *J. Am. Chem. Soc.* **2009**, *131*, 15647−15654.
(14) Moreno-García, P.; Gulcur, M.; Manrique, D. Z.; Pope, T.; Hong, W.; Kaliginedi, V.; Huang, C.; Batsanov, A. S.; Bryce, M. R.; Lambert, C. Single-Molecule conductance of functionalized oligoynes: Length dependence and junction evolution. *J. Am. Chem. Soc.* **2013**, *135*, 12228−12240.
(15) Meisner, J. S.; Kamenetska, M.; Krikorian, M.; Steigerwald, M. L.; Venkataraman, L.; Nuckolls, C. A single-molecule potentiometer. *Nano Lett.* **2011**, *11*, 1575−1579.
(16) Xu, W.; Leary, E.; Hou, S.; Sangtarash, S.; González, M. T.; Rubio-Bollinger, G.; Wu, Q.; Sadeghi, H.; Tejerina, L.; Christensen, K. E.; Agraït, N.; Higgins, S. J.; Lambert, C. J.; Nichols, R. J.; Anderson, H. L. Unusual length dependence of the conductance in cumulene molecular wires. *Angew. Chem., Int. Ed.* **2019**, *58*, 8378−8382.
(17) Zang, Y.; Fu, T.; Zou, Q.; Ng, F.; Li, H.; Steigerwald, M. L.; Nuckolls, C.; Venkataraman, L. Cumulene wires display increasing conductance with increasing length. *Nano Lett.* **2020**, *20*, 8415−8419.
(18) Gunasekaran, S.; Hernangómez-Pérez, D.; Davydenko, I.; Marder, S.; Evers, F.; Venkataraman, L. Near length-independent conductance in polymethine molecular wires. *Nano Lett.* **2018**, *18*, 6387−6391.
(19) Xu, W.; Leary, E.; Sangtarash, S.; Jirasek, M.; González, M. T.; Christensen, K. E.; Abellan Vicente, L.; Agraït, N.; Higgins, S. J.; Nichols, R. J. A Peierls transition in long polymethine molecular wires: Evolution of molecular geometry and single-molecule conductance. *J. Am. Chem. Soc.* **2021**, *143*, 20472−20481.
(20) Li, L.; Low, J. Z.; Wilhelm, J.; Liao, G.; Gunasekaran, S.; Prindle, C. R.; Starr, R. L.; Golze, D.; Nuckolls, C.; Steigerwald, M. L. Highly conducting single-molecule topological insulators based on mono-and di-radical cations. *Nat. Chem.* **2022**, *14*, 1061−1067.
(21) Li, L.; Louie, S.; Evans, A. M.; Meirzadeh, E.; Nuckolls, C.; Venkataraman, L. Topological radical pairs produce ultrahigh conductance in long molecular wires. *J. Am. Chem. Soc.* **2023**, *145*, 2492−2498.
(22) Li, J.; Peng, B.-J.; Li, S.; Tabor, D. P.; Fang, L.; Schroeder, C. M. Ladder-type conjugated molecules as robust multi-state single-molecule switches. *Chem.* **2023**, *9*, 2282.
(23) Zwick, P.; Dulić, D.; van der Zant, H. S. J.; Mayor, M. Porphyrins as building blocks for single-molecule devices. *Nanoscale* **2021**, *13*, 15500−15525.
(24) Leary, E.; Kastlunger, G.; Limburg, B.; Rincón-García, L.; Hurtado-Gallego, J.; González, M. T.; Bollinger, G. R.; Agrait, N.; Higgins, S. J.; Anderson, H. L.; Stadler, R.; Nichols, R. J. Long-lived charged states of single porphyrin-tape junctions under ambient conditions. *Nanoscale Horiz.* **2021**, *6*, 49−58.
(25) Schwarz, F.; Kastlunger, G.; Lissel, F.; Egler-Lucas, C.; Semenov, S. N.; Venkatesan, K.; Berke, H.; Stadler, R.; Lörtscher, E. Field-induced conductance switching by charge-state alternation in organometallic single-molecule junctions. *Nat. Nanotechnol.* **2016**, *11*, 170−176.
(26) Schwarz, F.; Koch, M.; Kastlunger, G.; Berke, H.; Stadler, R.; Venkatesan, K.; Lörtscher, E. Charge transport and conductance switching of redox-active azulene derivatives. *Angew. Chem., Int. Ed.* **2016**, *55*, 11781−11786.
(27) Migliore, A.; Nitzan, A. Nonlinear charge transport in redox molecular junctions: A Marcus perspective. *ACS Nano* **2011**, *5*, 6669−6685.
(28) Migliore, A.; Nitzan, A. Irreversibility and hysteresis in redox molecular conduction junctions. *J. Am. Chem. Soc.* **2013**, *135*, 9420−9432.
(29) Keane, Z. K.; Ciszek, J. W.; Tour, J. M.; Natelson, D. Three-terminal devices to examine single-molecule conductance switching. *Nano Lett.* **2006**, *6*, 1518−1521.
(30) Li, J.; et al. Room-temperature logic-in-memory operations in single-metallofullerene devices. *Nat. Mater.* **2022**, *21*, 917−923.
(31) Guo, Y.; Yang, C.; Zhou, S.; Liu, Z.; Guo, X. A single-molecule memristor based on an electric-field-driven dynamical structure reconfiguration. *Adv. Mater.* **2022**, *34*, No. 2204827.
(32) Millar, D.; Venkataraman, L.; Doerrer, L. H. Efficacy of Au−Au contacts for scanning tunneling microscopy molecular conductance measurements. *J. Phys. Chem. C* **2007**, *111*, 17635−17639.
(33) Chen, W.; Widawsky, J. R.; Vázquez, H.; Schneebeli, S. T.; Hybertsen, M. S.; Breslow, R.; Venkataraman, L. Highly conducting

https://doi.org/10.1021/jacs.3c07734
J. Am. Chem. Soc. XXXX, XXX, XXX−XXX

π-conjugated molecular junctions covalently bonded to gold electrodes. *J. Am. Chem. Soc.* **2011**, *133*, 17160−17163.
(34) Cheng, Z.-L.; Skouta, R.; Vazquez, H.; Widawsky, J. R.; Schneebeli, S.; Chen, W.; Hybertsen, M. S.; Breslow, R.; Venkataraman, L. *In situ* formation of highly conducting covalent Au−C contacts for single-molecule junctions. *Nat. Nanotechnol.* **2011**, *6*, 353−357.
(35) Pla-Vilanova, P.; Aragonès, A. C.; Ciampi, S.; Sanz, F.; Darwish, N.; Diez-Perez, I. The spontaneous formation of single-molecule junctions via terminal alkynes. *Nanotechnology* **2015**, *26*, No. 381001.
(36) Olavarria-Contreras, I. J.; Perrin, M. L.; Chen, Z.; Klyatskaya, S.; Ruben, M.; Van Der Zant, H. S. C−Au Covalently bonded molecular junctions using nonprotected alkynyl anchoring groups. *J. Am. Chem. Soc.* **2016**, *138*, 8465−8469.
(37) Bejarano, F.; Olavarria-Contreras, I. J.; Droghetti, A.; Rungger, I.; Rudnev, A.; Gutiérrez, D.; Mas-Torrent, M.; Veciana, J.; Van Der Zant, H. S.; Rovira, C. Robust organic radical molecular junctions using acetylene terminated groups for C−Au bond formation. *J. Am. Chem. Soc.* **2018**, *140*, 1691−1696.
(38) Tanaka, Y.; Kato, Y.; Tada, T.; Fujii, S.; Kiguchi, M.; Akita, M. Doping" of polyyne with an organometallic fragment leads to highly conductive metallapolyyne molecular wire. *J. Am. Chem. Soc.* **2018**, *140*, 10080−10084.
(39) Pera, G.; Martín, S.; Ballesteros, L. M.; Hope, A. J.; Low, P. J.; Nichols, R. J.; Cea, P. Metal−molecule−metal junctions in Langmuir−Blodgett Films using a new linker: trimethylsilane. *Chem.—Eur. J.* **2010**, *16* (45), 13398−13405.
(40) Marqués-González, S.; Yufit, D. S.; Howard, J. A.; Martín, S.; Osorio, H. M.; Garcia-Suarez, V. M.; Nichols, R. J.; Higgins, S. J.; Cea, P.; Low, P. J. Simplifying the conductance profiles of molecular junctions: The use of the trimethylsilylethynyl moiety as a molecule−gold contact. *Dalton Trans.* **2013**, *42*, 338−341.
(41) Milan, D. C.; Al-Owaedi, O. A.; Oerthel, M.-C.; Marqués-González, S.; Brooke, R. J.; Bryce, M. R.; Cea, P.; Ferrer, J.; Higgins, S. J.; Lambert, C. J. Solvent dependence of the single molecule conductance of oligoyne-based molecular wires. *J. Phys. Chem. C* **2016**, *120*, 15666−15674.
(42) Ferradás, R. R.; Marqués-González, S.; Osorio, H. M.; Ferrer, J.; Cea, P.; Milan, D. C.; Vezzoli, A.; Higgins, S. J.; Nichols, R. J.; Low, P. J. Low variability of single-molecule conductance assisted by bulky metal−molecule contacts. *RSC Adv.* **2016**, *6*, 75111−75121.
(43) Al-Owaedi, O. A.; Bock, S.; Milan, D. C.; Oerthel, M.-C.; Inkpen, M. S.; Yufit, D. S.; Sobolev, A. N.; Long, N. J.; Albrecht, T.; Higgins, S. J. Insulated molecular wires: Inhibiting orthogonal contacts in metal complex based molecular junctions. *Nanoscale* **2017**, *9*, 9902−9912.
(44) Hong, W.; Li, H.; Liu, S.-X.; Fu, Y.; Li, J.; Kaliginedi, V.; Decurtins, S.; Wandlowski, T. Trimethylsilyl-terminated oligo(phenylene ethynylene)s: An approach to single-molecule junctions with covalent Au−C σ-bonds. *J. Am. Chem. Soc.* **2012**, *134*, 19425−19431.
(45) Fu, Y.; Chen, S.; Kuzume, A.; Rudnev, A.; Huang, C.; Kaliginedi, V.; Baghernejad, M.; Hong, W.; Wandlowski, T.; Decurtins, S.; Liu, S.-X. Exploitation of desilylation chemistry in tailor-made functionalization on diverse surfaces. *Nat. Commun.* **2015**, *6*, 6403.
(46) Feilchenfeld, H.; Weaver, M. J. Binding of alkynes to silver, gold, and underpotential deposited silver electrodes as deduced by surface-enhanced raman spectroscopy. *J. Phys. Chem.* **1989**, *93*, 4276−4282.
(47) Sedghi, G.; Sawada, K.; Esdaile, L. J.; Hoffmann, M.; Anderson, H. L.; Bethell, D.; Haiss, W.; Higgins, S. J.; Nichols, R. J. Single molecule conductance of porphyrin wires with ultralow attenuation. *J. Am. Chem. Soc.* **2008**, *130*, 8582−8583.
(48) Li, Z.; Park, T.-H.; Rawson, J.; Therien, M. J.; Borguet, E. Quasi-Ohmic single molecule charge transport through highly conjugated *meso*-to-*meso* ethyne-bridged porphyrin wires. *Nano Lett.* **2012**, *12*, 2722−2727.
(49) Katsonis, N.; Marchenko, A.; Fichou, D.; Barrett, N. Investigation on the nature of the chemical link between acetylenic organosilane self-assembled monolayers and Au (111) by means of synchrotron radiation photoelectron spectroscopy and scanning tunneling Microscopy. *Surf. Sci.* **2008**, *602*, 9−16.
(50) Katsonis, N.; Marchenko, A.; Taillemite, S.; Fichou, D.; Chouraqui, G.; Aubert, C.; Malacria, M. A molecular approach to self-assembly of trimethylsilylacetylene derivatives on gold. *Chem.—Eur. J.* **2003**, *9*, 2574−2581.
(51) Sahoo, A. K.; Nakamura, Y.; Aratani, N.; Kim, K. S.; Noh, S. B.; Shinokubo, H.; Kim, D.; Osuka, A. Synthesis of brominated directly fused diporphyrins through gold(III)-mediated oxidation. *Org. Lett.* **2006**, *8*, 4141−4144.
(52) Akihiko, T.; Atsuhiro, O. Fully conjugated porphyrin tapes with electronic absorption bands that reach into infrared. *Science* **2001**, *293*, 79−82.
(53) Ikeda, T.; Aratani, N.; Osuka, A. Synthesis of extremely π-extended porphyrin tapes from hybrid *meso-meso* linked porphyrin arrays: An approach towards the conjugation length. *Chem.—Asian J.* **2009**, *4*, 1248−1256.
(54) Torras, J.; Casanovas, J.; Aleman, C. Reviewing extrapolation procedures of the electronic properties on the π-conjugated polymer limit. *J. Phys. Chem. A* **2012**, *116*, 7571−7583.
(55) Cuevas, J. C.; Scheer, E. *Molecular electronics: An introduction to theory and experiment*; World Scientific, 2010.
(56) We attempted to separate the different shaped traces using a *k*-means clustering algorithm, however, this proved unsuccessful as we found that the algorithm did not effectively distinguish 'V' shaped from 'U' shaped traces.
(57) Zotti, L. A.; Kirchner, T.; Cuevas, J.-C.; Pauly, F.; Huhn, T.; Scheer, E.; Erbe, A. Revealing the role of anchoring groups in the electrical conduction through single-molecule junctions. *Small* **2010**, *6*, 1529−1535.
(58) Wagner, S.; Kisslinger, F.; Ballmann, S.; Schramm, F.; Chandrasekar, R.; Bodenstein, T.; Fuhr, O.; Secker, D.; Fink, K.; Ruben, M.; Weber, H. B. Switching of a coupled spin pair in a single-molecule junction. *Nat. Nanotechnol.* **2013**, *8*, 575−579.
(59) Chen, Z.; Deng, J.-R.; Hou, S.; Bian, X.; Swett, J. L.; Wu, Q.; Baugh, J.; Bogani, L.; Briggs, G. A. D.; Mol, J. A.; Lambert, C. J.; Anderson, H. L.; Thomas, J. O. Phase-coherent charge transport through a porphyrin nanoribbon. *J. Am. Chem. Soc.* **2023**, *145*, 15265−15274.

https://doi.org/10.1021/jacs.3c07734
J. Am. Chem. Soc. XXXX, XXX, XXX−XXX